Journal of Volcanology and Geothermal Research 231–232 (2012) 61–71

Contents lists available at SciVerse ScienceDirect

Journal of Volcanology and Geothermal Research

journal homepage: www.elsevier.com/locate/jvolgeores

Deep-sea ash layers reveal evidence for large, late Pleistocene and Holocene explosive activity from Sumatra, Indonesia

Morgan J. Salisbury [a,*], Jason R. Patton [a], Adam J.R. Kent [a], Chris Goldfinger [a], Yusuf Djadjadihardja [b], Udrekh Hanifa [b]

[a] College of Earth, Ocean, and Atmospheric Sciences, Oregon State University, 104 Wilkinson Hall, Corvallis, OR 97331-5506, USA
[b] Bandan Penghajian Dan Penerapan Teknologi BPPT 2nd Building, 19th Floor, Jl.MH. Thamrin 8, Jakarta 10340, Indonesia

ARTICLE INFO

Article history:
Received 1 August 2011
Accepted 22 March 2012
Available online 30 March 2012

Keywords:
Tephra correlation
Sumatra
Volcanism
Marine tephras
Explosive volcanism

ABSTRACT

Deep-sea tephra layers sampled from sediment cores collected within, and adjacent to the Sunda trench of offshore Sumatra reveal evidence for five previously undocumented, and apparently large (minimum volume >0.6–>6.3 km^3; volcanic explosivity index values of 4–5) explosive eruptions over the last ~31,000 years, with a presumptive source of mainland Sumatra. Chemical analysis of glass shards and ^{14}C age constraints are used to distinguish the five tephra layers, as well as a sixth that likely correlates with the Youngest Toba tuff (YTT). The tephra layers are labeled V-1 through V-6 relative to their north-to-south positioning along the Sunda trench. The three tephra layers taken from cores west of central Sumatra (V-3, V-4, V-5) are well-constrained by ^{14}C age determinations, whereas less reliable sedimentation-rate estimates are available for the northern (V-1, V-2) and southern (V-6) tephra layers. Deposition of the northernmost tephra, layer V-1, was likely accompanied by seismicity as two chemically indistinguishable tephras are separated by 12 cm of course-grained turbidite. Layer V-2 shows a strong chemical resemblance to the YTT and age estimates do not rule out the correlation. With the exception of a likely correlation with the YTT, no other correlations were made between the tephras analyzed in this study with the marine or terrestrial record from the published literature. The most frequent, widespread, and youngest marine tephra layers were found in the central region of the study area. Layers V-3, V-4, and V-5 were all deposited within the last 17 thousand years with minimum eruptive volumes of >0.6 to >5.2 km^3. A complex depositional sequence of layer V-6 is estimated at ~27.5 ka, and may be associated with Late Pleistocene ignimbrite volcanism of southern Sumatra. The ages and suggested minimum volumes represented by the deep-sea tephra layers are consistent with an active volcanic arc, and demonstrate the need for further terrestrial studies.

1. Introduction

The island of Sumatra, Indonesia comprises the majority of the western Sunda Arc, one of the most volcanically active regions on Earth. The Global Volcanism Program lists 35 active volcanoes on the island (average spacing of 50 km) with reported eruptive activity occurring at 13 centers during the past 100 years, in addition to fumarolic and other signs of activity at many sites (Smithsonian Institution, 2012). Consequently, much of the island's human population and infrastructure is at risk from volcanic activity. Despite the dangers, the known Holocene eruption history of Sumatra is almost entirely limited to historic eye-witness accounts of small-to-moderate explosive activity from the past few hundred years. This lack of information is partly attributable to difficulties in accessibility, coupled with extremely high erosion rates and dense vegetation in this equatorial region. However, many of Sumatra's stratovolcanoes are steeply-sloped with only minor vegetation suggesting a youthful and frequent eruption history (e.g. Gasparon, 2005), and the overall large number of volcanoes suggests that increased knowledge of Sumatran volcanism would be valuable for volcanic hazard assessments. In this study, we take advantage of the recent availability of a set of tephra-bearing deep-sea sediment cores to document a number of large, explosive, Late Pleistocene to Holocene volcanic eruptions from the Sumatran mainland.

In 2007, workers from Oregon State University, in collaboration with the Agency for Assessment and Application of Technology, Indonesia, participated in the Paleoquakes07 research cruise that included collection of 144 deep-sea cores of shallow (<5 m) marine sediments deposited along the Sumatra–Andaman plate boundary (Fig. 1, Table 1). Turbidites within the cores, from within the Sunda trench and the adjacent continental slope, reveal at least nineteen and as many as twenty-four subduction zone earthquakes over the past 7.5 ka between ~5°N to ~2°N (Patton et al., 2010). Within the intercalated hemipelagic

* Corresponding author. Tel.: +1 2084201925.
E-mail addresses: salisbum@geo.oregonstate.edu (M.J. Salisbury), jpatton@coas.oregonstate.edu (J.R. Patton), adam.kent@science.oregonstate.edu (A.J.R. Kent), gold@coas.oregonstate.edu (C. Goldfinger), iyung24@yahoo.com (Y. Djadjadihardja), udrekh@gmail.com (U. Hanifa).

0377-0273/$ – see front matter © 2012 Elsevier B.V. All rights reserved.
doi:10.1016/j.jvolgeores.2012.03.007

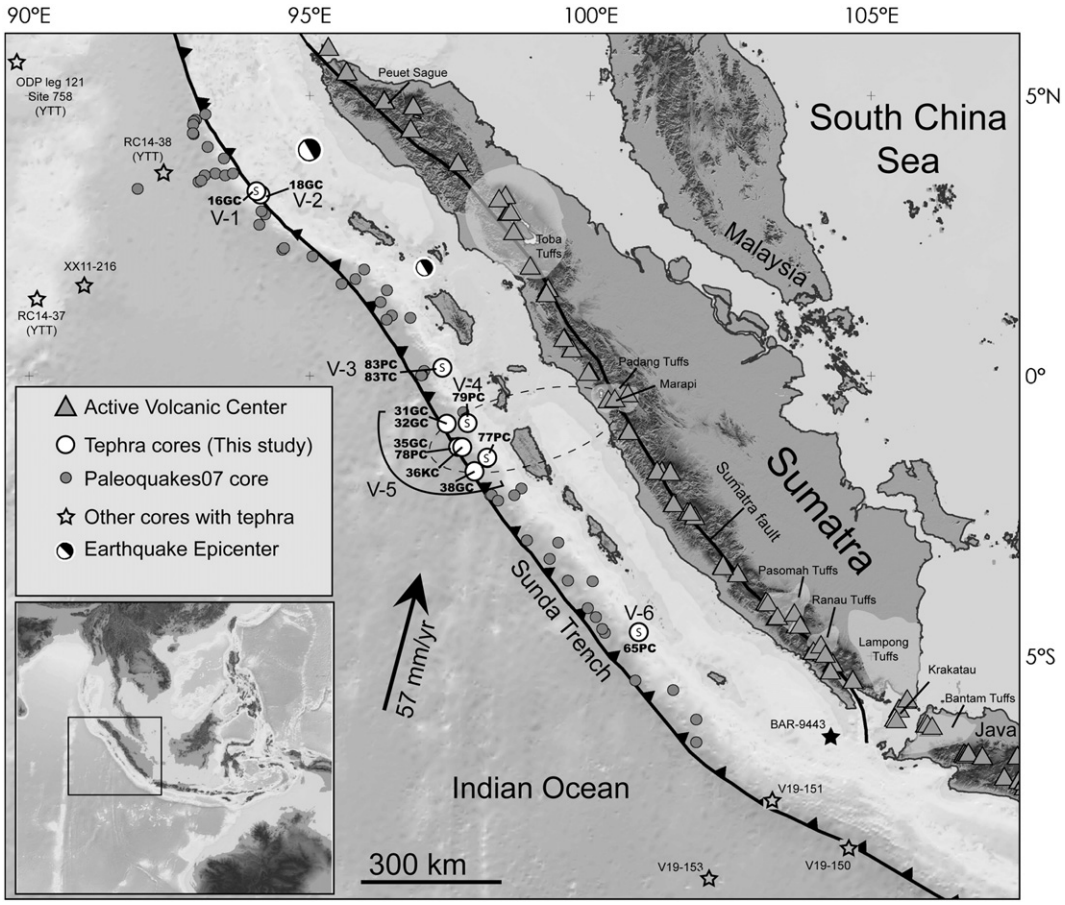

Fig. 1. Location of deep-sea marine cores analyzed in this study. Larger white circles represent cores in which tephra was identified and analyzed geochemically. Cores from the continental slope are identified with an "S". Smaller, light gray circles represent examined cores without identified tephra deposits. Individual volcanic units are labeled as V-1 through V-6 relative to north-to-south core location. A dashed line shows the minimum distribution ellipse used in volume calculations for unit V-5. Triangles represent active volcanoes of the west Sunda arc as identified by the Global Volcanism Program (Smithsonian Institution, 2011). Also shown are locations of deep-sea cores with tephra horizons analyzed by Ninkovich (1979) (open stars) and Beauregard (2001) (solid star). Bathymetry and topography data are from Smith and Sandwell (1997).

sediment and turbidites, tephra layers analyzed in the present study were identified in cores collected at distances of 200–300 km west of the modern Sumatran arc front.

In this study, we establish the composition, age constraints, and distribution of the newly discovered tephra layers and provide constraints on Late Pleistocene to Holocene eruptions capable of transporting

Table 1
Physical characteristics of deep-sea cores and tephra samples from Cruise RR0705.

Core		Lat.	Long.	Seafloor depth (m)	Tephra depth (cm)	Tephra thickness (cm)	Tephra sample #	Dominant shard type[b]	Avg. shard (μm)	EMP # analyses	LA-ICP-M # analyses	Spot size (μm)	Tephra layer designation
Num.	Type[a]												
16	GC	3.287	94.035	1911	146	4.0	SUM132	1 and 2	50	28	22	40	V-1
16	GC	3.287	94.035	1911	130	5.0	SUM134	1 and 2	50	37	21	40	V-1
18	GC	3.276	94.020	1820	222	5.0	SUM136	2	< 30	34	6	30	V-2
83	PC	0.130	97.361	3337	151	0.5	SUM049	1	90	32	27	70	V-3
83	TC	0.130	97.361	3337	203	1.3	SUM048	1	90	18	18	70	V-3
79	PC	–0.847	97.794	3833	165	3.5	SUM137	1	50	28	17	30	V-4
79	PC	–0.847	97.794	3833	303	8.0	SUM008	1	90	28	15	70	V-5
31	GC	–0.860	97.430	5420	84	2.7	SUM106	1	90	31	31	70	V-5
32	GC	–0.860	97.442	5435	43	2.3	SUM011	1	90	31	27	70	V-5
35	GC	–1.283	97.650	5455	110	3.4	SUM010	1	90	34	19	70	V-5
78	PC	–1.283	97.650	5455	243	3.9	SUM009	1	90	34	33	70	V-5
38	GC	–1.699	97.938	5511	144	1.0	SUM012	1	90	34	14	70	V-5
77	PC	–1.478	98.155	3778	120	1.5	SUM131	1	110	36	27	70	V-5
36	KC	–1.283	97.650	5455	15	1.5	SUM138	2	30	31	14	30	V-5
65	PC	–4.579	100.858	2751	436	n.d	SUM013	1 and 2	100	13	0	n.a.	V-6
65	PC	–4.579	100.858	2751	440.5	n.d	SUM014	1 and 2	100	12	0	n.a.	V-6
65	PC	–4.579	100.858	2751	441.7	n.d	SUM015	1 and 2	100	6	0	n.a.	V-6
65	PC	–4.579	100.858	2751	465.5	n.d	SUM016	1 and 2	100	43	33	70	V-6
65	PC	–4.579	100.858	2751	481.3	5.1	SUM017	1 and 2	100	7	0	n.a.	V-6
65	PC	–4.579	100.858	2751	486.3	6.1	SUM018	1 and 2	100	11	0	n.a.	V-6

[a]Core type: GC = gravity core; PC = piston core; TC = trigger core; KC = kasten core.
[b]Shard type 1 = micropumiceous, type 2 = bubble-wall or platy.
[c]n.d = not determined, reworked sediment.

and depositing volcanic ash several hundreds of kilometers from the Sumatran arc. We take advantage of recent advances in microbeam analysis of tephra by electron microprobe and laser ablation ICP-MS (LA-ICP-MS) (e.g. Pearce et al., 2007) that allow measurement of major and trace element chemistry of individual tephra particles to facilitate tephra correlation of distal volcanic layers (e.g. Adams, 1990; Ukstins Peate et al., 2003, 2005; Pearce et al., 2008). In addition to a likely correlation with the Youngest Toba tuffs (YTT), we identify at least five Late Pleistocene to Holocene eruptive deposits that do not correlate with known terrestrial eruptions. ^{14}C age determinations of foraminifera constrain the deposition age of tephra within cores taken from the shallower waters of the continental slope. These ages are further used to derive hemipelagic sedimentation rates that are extended to the cores from the Sunda trench that enable approximate estimates of the timing of deposition of tephra within the deeper, foraminifera-free trench environment. The most widespread of these eruptive deposits, layer V-5, is tightly constrained by ^{14}C age determinations at ~4.9 ka, suggesting a newly discovered Holocene eruption of potential significance for the historic record.

2. Regional setting

The Sunda arc is divided into western and eastern portions with respect to the Sunda Strait (Fig. 1). West of the strait, the Indo-Australian plate subducts obliquely beneath the pre-Cenozoic continental crust of Sumatra, whereas orthogonal subduction beneath younger, oceanic lithosphere occurs at the eastern plate boundary near Java and the Lesser Sunda Islands. The oblique convergence is partly accommodated by the Great Sumatran fault zone: a major strike-slip fault that follows the trace of the volcanic arc across the approximately 1700 km-long island and contributes to complex magmatic–tectonic relationships in the development of pull-apart basins and related caldera activity (e.g. van Bemmelen, 1949; Bellier and Sébrier, 1994). Forearc basins in western Sumatra are bound to the west by an accretionary complex partly emerged as the Mentawai islands, roughly 200 miles from the active arc. The continental shelf drops off sharply as it approaches the Sunda trench and reaches depths up to 6.5 km.

Magmatic activity on Sumatra has been ongoing throughout the Cenozoic (Bellon et al., 2004). Quaternary volcanism is dominantly characterized by large silicic tuffs from caldera systems and by intermediate-composition volcanism from stratovolcanoes of the frontal arc (Gasparon, 2005). Mafic volcanism is rare in this region, due in part to assimilation of Paleozoic continental crust and extensive crystal fractionation (e.g. Gasparon and Varne, 1995). Four major Pliocene to Quaternary pyroclastic deposits are recognized in Sumatra: the ~74 ka, 2700 km^3 Younger Toba tuffs (Rose and Chesner, 1987; Chesner et al., 1991) in the north, the Padang tuffs in the central region, and the Lampung and ~0.55 Ma Ranau tuffs (Bellier et al., 1999) in the south (Fig. 1). No radiometric ages are available for the Padang and Lampung tuffs. The southern silicic tuffs may further be related to extension caused by the clockwise rotation of Sumatra relative to Java since the Late Miocene (e.g. Ninkovich, 1976).

General accounts of the Quaternary eruption history are provided by van Bemmelen (1949), Westerveld (1952), Whitford (1975), Rock et al. (1982), and Gasparon (2005), among others, although few of the eruptions are well dated or characterized compositionally. Explosive activity in these reports is generally limited to short descriptions of large tuffaceous outcrops from the major caldera systems. Few studies have attempted to understand the eruptive characteristics of the stratovolcanoes on the Sumatran mainland despite the high frequency of observed historic activity. For example, at least seven volcanoes have experienced small-to-moderate explosive eruptions since the beginning of the 21st century (Smithsonian Institution, 2011), although very little is known about the Late Pleistocene to Holocene eruption history of these centers. Most of our knowledge of regional volcanism during this timeframe is related to Krakatau volcano, in the Sunda strait between the islands of Sumatra and Java. Krakatau is among the most active volcanoes in the region, exemplified by the 1883 eruption (volcanic explosivity index [VEI] = 6; Newhall and Self, 1982) that expelled 12.5 km^3 of dominantly rhyodacitic magma (Mandeville et al., 1996). Tephra dispersal studies from the marine environment have also been successful in revealing the large-scale explosive activity (erupted volumes of hundreds of km^3) from Sumatra and western Java. The YTT is found throughout the Northern Indian Ocean (e.g. Ninkovich and Donn, 1976; Ninkovich et al., 1978), the Central Indian Basin (Ninkovich, 1979; Pattan et al., 1999) and the South China Sea (Bühring and Sarnthein, 2000; Song et al., 2000). Dehn et al. (1991) identified several hundred tephra layers from Ocean Drilling Program site 758 (5°23.05′N, 90°21.67′E) in the northeast Indian Ocean, approximately halfway between northern Sumatra and the Indian mainland. Of these, 17 were greater than 1 cm and the youngest, a 34 cm thick deposit, correlates with the YTT. Ninkovich and Donn (1976) and Ninkovich (1979) identified Late Miocene to Recent deep-sea tephra layers from the Indian Ocean and describe three compositional regions with respect to the Indonesian archipelago: andesitic tephras offshore eastern Java and the Lesser Sunda Islands, dacitic tephras near the Sunda strait with a presumed source of Krakatau, and widespread rhyolitic tephras throughout the northern Indian Ocean.

The marine and terrestrial records described above provide only minimal estimates of the frequency and potential of Sumatran volcanism during the Late Pleistocene and Holocene, particularly for relatively smaller eruptions that do not provide tephra records over such extensive distances as observed for the YTT. High rates of erosion and extensive vegetative cover, coupled with limited volcanic research on the Sumatran mainland, has resulted in limited documentation of the moderate-to-large explosive eruptions in the 0.1–9 km^3 range (VEI = 4–5). In the present study, the deep-sea marine tephras allow us to begin to document the Late Pleistocene to Holocene tephra record and to bridge the gap between the older (>74 ka), larger (VEI ≥ 6) tephras, such as the YTT, found in cores at distances greater than 500 km from the arc (Ninkovich et al., 1978; Ninkovich, 1979; Dehn et al., 1991), and the small-to-moderate eruptions (VEI ≤ 3) that have been frequently witnessed in historical time (Smithsonian Institution, 2011).

3. Methods

3.1. Tephra sample collection

Of the 144 sediment cores collected by the PaleoQuakes07 cruise along an ~1600 km transect parallel to the Sunda trench, coherent and visually distinguishable tephra layers were found in 13 cores from 8 geographic localities (Fig. 1, Table 1). Core data including color imagery, computed tomography (CT) scans, magnetic susceptibility (MST), and density measurements are available for download in the Supplementary appendix (A.1). The tephra horizons were identified by their white to pink color and further distinguished by relatively high magnetic susceptibility and coarser grain sizes compared to hemipelagic sediment. Tephra thicknesses range from a few mm to at least 8 cm and display varying amounts of bioturbation, identified in the CT imagery. Small (<1 cm^3) samples were collected from the tephra horizons and rinsed in deionizied water to remove fine-grained hemipelagic sediment. The samples were dried, mounted in epoxy, and polished with grit paper and 1 μm alumina powder prior to microanalysis.

3.2. Geochronology

Age estimates for the deposition of tephra layers in this study are constrained through radiocarbon age determinations of planktic foraminifera and sedimentation rate based age estimates (Table 2). Planktic foraminifera are assumed to represent the age of the seawater that is most closely in ^{14}C equilibrium with the atmosphere. Planktic

Table 2
Estimated depositional ages for volcanic units based on radiocarbon ages and calculated sedimentation rates.

Tephra unit	Core number	Sed. rate (cm/ka)	Sed. rate error (cm/ka)	Age type[a]	Calendar age (years BP)[b,c]	Age error (years, 95%)
V-1	16GC	1.80	1.02	sed-rate	30,940	280
V-2	18GC	1.80	1.02	sed-rate	109,750	320
V-3	83PC	1.59	1.05	sed-rate	13,610	630
V-4	79PC	12.53	1.00	direct	1930	190
V-5	79PC	17.53	1.00	direct	4860	60
V-5[d]	77PC	7.22	1.00	sed-rate	5470	140
V-6	65PC	4.55	1.00	sed-rate	27,530	480

Radiocarbon concentrations are given as fractions of the Modern standard, $D^{14}C$, and conventional radiocarbon age, following the conventions of Stuiver and Polach (1977). Size-dependent sample preparation backgrounds have been subtracted, based on measurements of ^{14}C-free calcite.
All results have been corrected for isotopic fractionation according to the conventions of Stuiver and Polach (1977), with $d^{13}C$ values measured on prepared graphite using the AMS spectrometer. These can differ from $d^{13}C$ of the original material, if fractionation occurred during sample graphitization or the AMS measurement, and are not shown.
[a] "Direct" ages are tephras with ages directly underlying the deposit; "sed-rate" ages are determined using hemipelagic thickness and sedimentation rates (explained further in Section 3.2).
[b] Radiocarbon samples were analyzed at the Keck Carbon Cycle Accelerator Mass Spectroscopy Facility at Earth System Science Dept., UC Irvine (John Southon).
[c] Calibrated age ranges before A.D. 1950 according to Stuiver et al. (1998) calculated using marine reservoir correction ($\Delta R = 16$); errors reported to 95%.
[d] Preferred age for V-5 is from the better constrained core 79PC.

foraminifera were only available for select cores from the continental slope, where ocean floor depths are above the Carbonate Compensation Depth (CCD). Below the CCD, foraminiferid $CaCO_3$ tests dissolve faster than they are deposited. Foraminifera were sampled from hemipelagic sediment immediately underlying tephras, providing closely limiting maximum ages. Because the contact between the tephras and the overlying hemipelagite is often obscured by physical factors including bioturbation, the overlying sediment is not used to provide the minimum limiting ages. For ^{14}C dating, hemipelagic sediment samples were removed from the cores while avoiding the ~5 mm of material nearest the core walls to avoid visible or undetected deformation and friction drag along the core walls. Samples were freeze-dried to separate clay particles, rinsed through a sieve, and then washed in a dilute Calgon (sodium hexametaphosphate) solution to keep fine particles in suspension. The samples were then sieved at 125 μm and oven dried. Typically 25–50 individual planktic foraminifera (depending on size/weight)

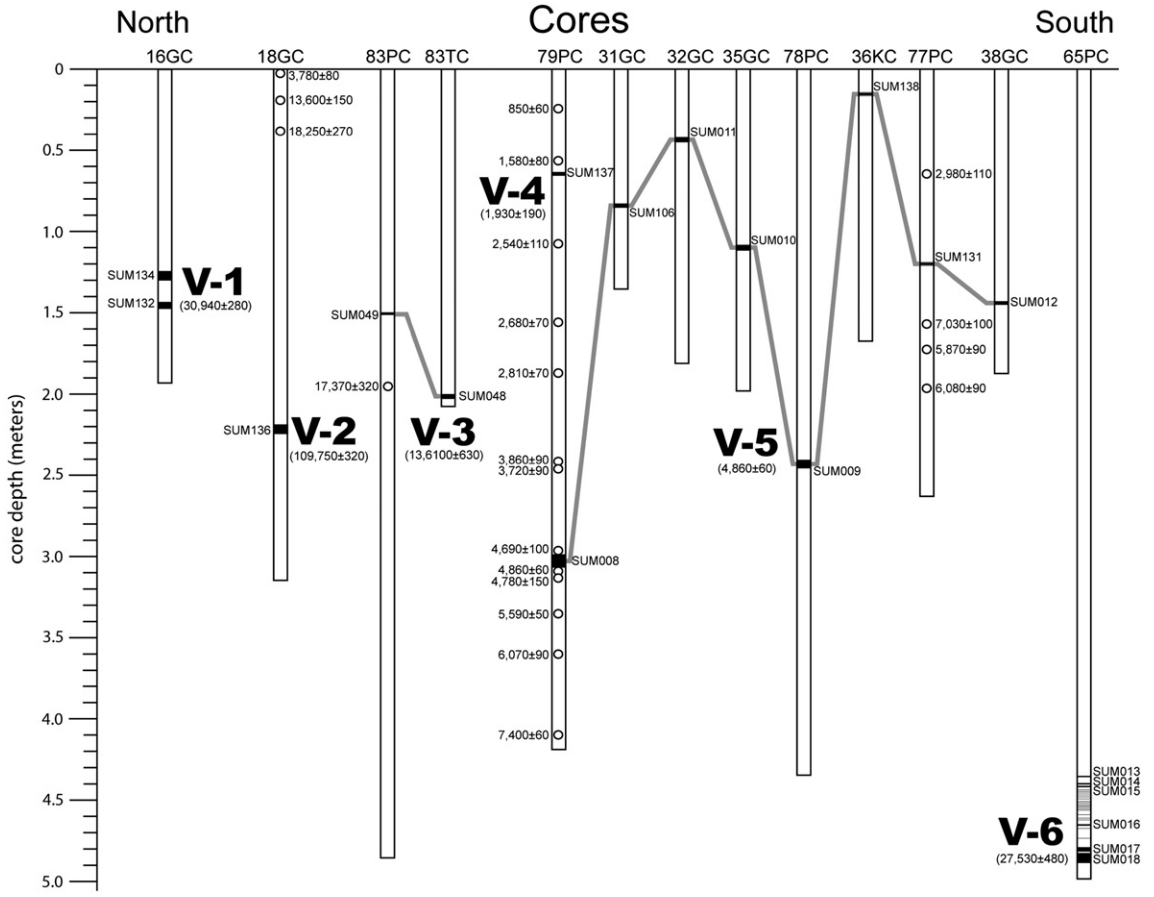

Fig. 2. Cores are plotted vs. depth in meters. Tephra layer sample positions are designated by their sample name (e.g. SUM00X). Ages are cal yr BP. Direct ^{14}C age sample locations are plotted as circles and their calibrated ages are listed with 95% error. Sedimentation-rate derived depositional ages are listed with 95% error in parenthesis beneath each layer designation. See Fig. 1 for core locations. Gray tie-line shows correlation of tephra layers between the cores.

were identified (as planktonic, not benthic) then removed from the dried, >125 μm size fraction using a fine sable brush moistened with distilled water.

Foraminiferid sample ages were determined using Accelerator Mass Spectrometry (AMS) methods at the Keck AMS facility at University of California, Irvine and calibrated using OxCal v4.1.5 (Bronk Ramsey, 2009; Reimer et al., 2009) and a marine reservoir correction of 16 ± 11 years was made using the Marine Reservoir Correction Database (Stuiver and Braziunas, 1993). Only two delta R values are available for the Sumatra area, and while constraints are sparse in this correction, in this study we correlate marine sites to other nearby marine sites wherever possible, thus we assume the local correlations are valid, although absolute ages may contain additional uncertainty. The calculations include lab uncertainties and no lab multipliers were applied to the data (Taylor et al., 1996). The radiocarbon ages are reported in years before present (BP, measured from 1950) with a 95% error (Bronk Ramsey, 2009).

Tephra depositional ages without underlying foraminifera are estimated using hemipelagic sedimentation rates calculated using ^{14}C data from above the tephra layer or from the nearest available cores with age data. Sedimentation rates are calculated by dividing the sediment thickness by the underlying ^{14}C age. Sedimentation rate calculations assume that the top of the core has an age of 0 years, which we consider reasonable in this case given the presence of oxidation of the surficial sediments. ^{210}Pb analyses were not conducted for each core. For cores with multiple ^{14}C ages, we calculate moving average sedimentation rates. To estimate the age of a tephra with no underlying datable material, the total overlying hemipelagic thickness is divided by the sedimentation rate, in some cases calculated from a nearby core. Although this method introduces unconstrained variables and assumptions, further described below, we consider the sedimentation rate-based ages to provide meaningful constraints on the depositional ages of these tephras. Based on core lithostratigraphy, MST data, CT and visual imagery, non-tephra sediment type is interpreted as hemipelagic or turbiditic. Turbidites are assumed to represent instant deposition so only hemipelagic sediment is used to calculate sedimentation rates. As discussed above in relation to the tephras, the uncertainty with determining the position of the upper contacts of the turbidites introduces error into the total sediment thickness used to calculate the sedimentation rates. Another source of unconstrained error is involved with the assumption that the hemipelagic sediment rate is the same for both the foraminifera-bearing slope cores and those of the Sunda trench. The reported sedimentation rate derived age error includes propagated root mean square error from thickness estimates in addition to error from ^{14}C age determinations used in their construction.

3.3. Glass morphology

Material from each tephra layer is generally fine-grained (<200 μm) and consists primarily of volcanic glass with lesser amounts of mineral fragments and organic material. Glass shards (Fig. 3) are typically colorless and clear, and contain numerous vesicles (micropumiceous) or are elongate with curvaceous edges and lacking in internal vesicles (bubble-wall or platy). Micropumiceous glass shards dominate most tephra layers (Table 1). No discoloration or visual chemical alteration was identified on the glass shards during inspection with the petrographic microscope.

3.4. Electron microprobe analysis

Major and minor oxide compositions of ~528 glass shards from 20 tephra samples (avg. = 26 shards/sample) were determined by electron microprobe analysis (EMPA) using a Cameca SX-100 electron microprobe at Oregon State University with an accelerating voltage of 15 kV and an electron beam of 15 nA, defocused to 10 μm to prevent volatile loss. Accuracy and precision were monitored for the majority

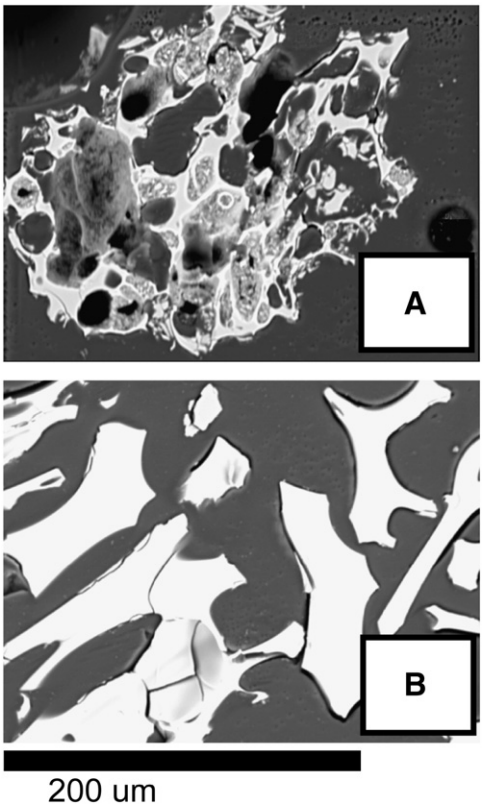

Fig. 3. Electron microprobe backscatter images of: (A) typical micropumiceous glass shard (SUM008) and (B) bubble-wall junction, or platy, glass shards (SUM016). No compositional differences were observed between shards of varying morphology within individual tephra samples.

of the samples through periodic analysis of rhyolite glass standard RHYO from the United States Museum of Natural History. The relative standard deviation of major elements (>1.0 wt.%) of all standard analyses was <1% for SiO_2 and Al_2O_3, <3% for K_2O and Na_2O, and <12% for FeO* and MgO. For minor elements (0.1–1.0 wt.%) relative standard deviation was <9% for CaO, TiO_2, and Cl. Throughout the rest of the paper we refer to both minor and major elements analyzed by EMPA as major elements. Analytical totals are consistent within each tephra sample and only those greater than 95% are considered in this study. Analyzed glass shards typically varied in size from ~30 μm to 200 μm in diameter. Most shards were measured twice and are typically homogenous with internal SiO_2 variations <1 wt.%. Complete chemical analyses are available in the digital appendix (B.1).

3.5. LA-ICP-MS analysis

Trace elements of a subset (324 analyses, B.1) of the same glass shards as measured by EMPA were measured by LA-ICP-MS in the W.M. Keck Collaboratory for Plasma Spectrometry at Oregon State University using a NewWave DUV 193 μm ArF Excimer laser and VG PQ ExCell Quadrupole ICP-MS following techniques outlined in Kent et al. (2004). Laser ablation spot size varied from 30 to 70 μm with the lower value necessary for smaller shard sizes of some of the samples (Table 1). Ablation was performed using He as the carrier gas, and He plus ablated particulates were mixed with the Ar nebulizer gas flow immediately prior to the plasma torch. Background count rates were measured for 30 s prior to ablation and subtracted directly from count rates measured during ablation. Plasma torch conditions were optimized so that oxide production (estimated from measured ThO/Th ratios) was <1–2%. Abundances of individual trace elements

were calculated relative to USGS glass standard BCR-2G. ^{29}Si was used as an internal standard in conjunction with SiO_2 contents measured by the electron microprobe. BHVO-2G and NIST-612 glasses were also analyzed to monitor accuracy and precision. Repeat analyses of NIST-612 showed differences from the accepted composition of <10% for Rb, Sr, Ba, Nb, Ta, Pb, U, Sc, La, Ce, Pr, Nd, and Sm and 10–25% for Y, Zr, Hf, Th, Eu, Gd, Dy, Er, and Yb. Relative standard deviation for the repeat analyses of NIST-612 varied by <15% for Rb, Sr, Ba, Nb, Pb, U, and Ce and ≤25% for all other trace elements.

3.6. Statistical correlation of glass shard tephra samples

Glass shards have been shown to be well-suited for correlative study as they typically undergo only minor hydration or ion-exchange with respect to both major (e.g. Ninkovich, 1979) and trace elements (e.g. Ukstins Peate et al., 2003) even when subjected to long residence times in seawater. The similarity of glass compositions from each sampled tephra in this study is described by the statistical distance function as used by Perkins et al. (1995, 1998):

$$D^2_{\text{calculated}} = \sum_{k=1}^{n} (x_{k1} - x_{k2})^2 / \left(\sigma^2_{k1} + \sigma^2_{k2}\right)$$

where n is the number of elements used in the comparison, x_{k1} and x_{k2} are the average concentrations of the kth element of the two samples, and σ_{k1} and σ_{k2} are the standard deviations of the kth element in each sample. The lower the value of $D^2_{\text{calculated}}$ the greater the probability that the two samples are from the same population with zero as the ideal value for a chemically identical pair. Because of the different methods used in data collection, we calculate D^2 values separately for a suite of 9 major (and minor) elements and a suite of 22 trace elements. The distribution of D^2 follows the chi^2 distribution and from this a critical value (D^2_{critical}) can be established to form a theoretical cutoff where samples can be said to be sufficiently similar to be considered correlatives. At the 95% confidence level, D^2_{critical} is 16.9 for 9 variables and 33.9 for 22 variables.

4. Correlations of marine tephra layers

We use combined data from the chemical composition of individual glass shards, ^{14}C age constraints, and the stratigraphic relations of core sedimentological features to establish individual tephra layers of offshore western Sumatra. From this correlative scheme, six distinct volcanic tephra layers are identified and are named based on their north (V-1) to south (V-6) latitudinal positioning off the Sumatra mainland (Figs. 1 and 2). ^{14}C age determinations are shown in Table 2. Statistical distance values for all sample pair combinations of average glass compositions are reported for both major and trace elements in Table 3. Average unit compositions and standard deviations of compositional data for each of the tephra layers are shown in Table 4.

Each of the six layers is interpreted as a single eruptive phase from a terrestrial source, with the western Sunda arc the most likely due to its proximity and glass compositions consistent with arc magmatism. The glass shards define a compositional spectrum of calc-alkaline, medium-K to high-K, andesites to rhyolites (Fig. 4). Trace element analysis reveals a relative enrichment of large ion lithophile elements compared to high field strength elements and a slight to moderate

Table 3
Statistical distance (SD) values for Sunda trench and adjacent slope.

SD for 9 oxides analyzed by EMP. D-critical = 16.9

	SUM008	SUM009	SUM010	SUM011	SUM012	SUM016	SUM048	SUM049	SUM106	SUM131	SUM132	SUM134	SUM136	SUM137	SUM138
SUM009	3.45														
SUM010	0.84	2.50													
SUM011	0.60	1.00	0.36												
SUM012	1.66	2.06	0.17	0.45											
SUM016	143	93	84	59	104										
SUM048	248	105	159	117	169	865									
SUM049	208	96	141	107	144	598	0.97								
SUM106	0.5	2.2	1.1	0.6	1.6	117	205	173							
SUM131	7.0	3.0	7.4	6.0	8.5	81	95	84	4.8						
SUM132	137	110	94	72	113	94	710	526	117	99					
SUM134	131	93	85	62	106	230	831	569	111	93	0.53				
SUM136	164	90	94	64	118	69	853	597	125	89	142	152			
SUM137	36	15	25	20	26	165	64	55	28	9.5	174	182	224		
SUM138	5.8	2.8	6.9	5.8	8.1	58	90	77	4	0.14	73	72	71	10	
YTT[a]	175	94	106	69	135	47	847	585	137	83	83	99	26	230	62

SD values for 22 trace elements analyzed by ICP-MS. D-critical = 33.9

	SUM008	SUM009	SUM010	SUM011	SUM012	SUM016	SUM048	SUM049	SUM106	SUM131	SUM132	SUM134	SUM136	SUM137	SUM138
SUM009	13.3														
SUM010	2.5	11.6													
SUM011	3.5	8.5	3.5												
SUM012	2.5	6.8	2.1	2.7											
SUM016	252	128	225	133	127										
SUM048	133	56	93	77	71	399									
SUM049	116	51	78	68	59	375	2.41								
SUM106	5.1	15.3	4.6	4.2	7.4	166	95	83							
SUM131	35.0	42.1	28.3	31.3	31.4	185	57	49	22.3						
SUM132	116	121	117	110	95	140	332	333	102	117					
SUM134	91	97	98	88	83	113	237	233	85	83	2.5				
SUM136	140	102	133	102	100	73	162	143	103	91	64	57			
SUM137	85	55	71	64	58	196	19	14	81	42	211	180	124		
SUM138	43.3	57.6	39.7	41.9	42.0	148	78	71	33.0	7.9	85	75	66	70	
YTT[a]	140	71	129	79	76	42	120	91	89	69	47	46	29	74	60

Note: shaded values below D-critical.
[a]YTT values averaged from glass shards analysis of Chesner and Luhr (2010).

Table 4
Average major-oxide (un-normalized) and trace element compositions of individual tephra units.

Layer	V-1		V-2		V-3		V-4		V-5		V-6	
n	65		34		50		28		259		36	
EMP (wt.%)	avg.	s.d.	avg.	s.d.	avg.	s.d.	avg.	s.d.	avg.	s.d.	avg.	s.d.
SiO_2	73.7	0.5	73.9	0.4	62.5	1.0	69.3	1.7	71.7	1.8	75.2	0.5
Al_2O_3	12.4	0.3	12.5	0.2	17.3	0.7	15.4	0.9	14.6	0.8	12.4	0.2
CaO	1.19	0.14	0.77	0.10	5.01	0.42	3.11	0.74	2.43	0.57	0.70	0.02
MgO	0.19	0.01	0.06	0.01	2.02	0.33	0.88	0.23	0.54	0.23	0.12	0.00
FeO*	1.0	0.0	0.9	0.1	5.8	0.6	2.9	0.5	2.1	0.4	0.8	0.0
TiO_2	0.16	0.01	0.06	0.01	0.82	0.08	0.56	0.07	0.36	0.08	0.12	0.01
MnO	0.05	0.01	0.06	0.02	0.15	0.02	0.09	0.02	0.06	0.02	0.08	0.01
K_2O	4.4	0.1	5.0	0.2	2.4	0.2	2.6	0.2	3.2	0.3	4.2	0.1
Na_2O	2.2	0.1	2.4	0.1	3.6	0.6	3.5	0.4	2.5	0.6	2.4	0.3
Cl	0.23	0.01	0.14	0.02	0.11	0.01	0.17	0.02	0.13	0.01	0.18	0.01
SO_2	0.01	0.01	0.00	0.00	0.02	0.01	0.03	0.02	0.01	0.01	0.00	0.00
F	0.02	0.02	0.04	0.02	0.04	0.02	0.03	0.02	0.01	0.02	0.01	0.01
Total	95.6	0.6	95.8	0.5	99.8	0.8	98.5	1.4	97.7	1.5	96.1	0.8
LA-ICP-MS (ppm)	43		6		49		17		180		33	
n	avg.	s.d.	avg.	s.d.	avg.	s.d.	avg.	s.d.	avg.	s.d.	avg.	s.d.
Rb	171	7	269	24	74	6	79	11	134	14	186	5
Sr	206	46	52	21	352	56	291	78	214	51	56	8
Ba	969	80	475	194	429	35	455	55	538	64	432	25
Y	19	4	64	20	39	10	63	17	30	10	20	2
Zr	177	28	144	15	219	46	270	63	310	84	101	9
Nb	12	1	21	4	7	1	6	1	8	1	6	1
Hf	5.7	1.9	4.3	2.2	5.6	1.6	7.7	2.8	7.9	2.5	3.4	0.9
Ta	1.6	0.4	2.3	1.2	0.5	0.1	0.5	0.3	0.7	0.2	0.6	0.1
Pb	34.3	10.8	39.7	4.4	24.5	6.4	18.6	4.1	22.5	6.0	28.2	3.6
Th	44.5	7.6	59.5	14.8	7.8	1.6	14.2	3.1	15.2	4.4	29.1	3.0
U	4.0	0.7	5.9	2.2	1.7	0.3	2.0	0.5	2.1	0.4	5.5	0.5
Sc	6.6	3.2	8.7	2.4	16.5	3.2	16.5	4.6	7.8	3.4	5.6	1.1
La	51.1	7.1	46.6	11.3	22.3	3.3	21.4	4.1	32.5	6.4	28.8	2.8
Ce	60.3	5.2	62.7	13.1	44.6	3.7	36.5	3.6	58.8	5.3	48.8	2.7
Pr	6.2	1.1	7.9	0.9	5.7	0.6	5.5	1.2	7.0	1.0	5.1	0.5
Nd	20.7	4.7	37.8	10.1	25.8	3.3	26.8	5.7	27.1	5.9	17.1	2.3
Sm	3.1	1.1	6.7	2.5	6.3	1.3	7.1	1.2	5.1	1.4	2.8	0.9
Eu	0.6	0.3	0.5	0.2	1.4	0.3	1.5	0.5	1.0	0.3	0.3	0.1
Gd	3.1	1.5	6.6	3.6	6.4	1.7	9.9	3.2	4.7	1.9	2.8	1.1
Dy	2.6	1.2	6.3	1.6	6.4	1.7	9.1	2.9	4.5	1.5	3.2	1.1
Er	1.8	0.8	6.8	2.7	4.2	1.1	6.5	1.5	3.0	1.1	1.9	0.6
Yb	2.1	0.8	5.4	3.9	4.1	0.9	7.3	2.6	3.1	1.1	2.2	0.5

enrichment of light REE relative to heavy REE, and negative Eu anomalies.

Major oxide analysis of glass shards reveals three distinct compositional groups of increasing silica concentrations (Groups 1–3 in Fig. 4) and forms the chemical framework for establishing correlations of the tephra layers. Group 1 shards have SiO_2 contents between ~60–65 wt.%, Group 2 have ~68–76 wt.% SiO_2 and Group 3 have $SiO_2 >$ ~76 wt.%. Group 2 shards preserve the most coherent linear trends of major elements, with the exception of Na_2O (Fig. 4f) suggesting that Na-loss occurred via secondary shard hydration and/or during EMPA analysis. Samples containing both micropumiceous and platy shards show no significant compositional differences between the two shard types. Trace element concentrations further distinguish the tephra samples and reveal greater detail than provided by the major element data alone (Figs. 5 and 6), consistent with the typically larger variation evident in trace elements in igneous rocks as their concentrations are less likely to be buffered by phase equilibria. Most high field strength elements (HFSE), such as Y, Zr, Hf, Th, and La, exhibit stronger positive correlations with each other (Fig. 5c–d) than the large ion lithophile elements (LILE), although both HFSE and LILE show similar compositional ranges.

4.1. Group 1 tephra correlations

Group 1 glass shards were sampled from a piston core (PC) and gravity core (GC) collected only a few meters apart (Table 1) and are interpreted to represent a single tephra layer, V-3. The tephras in two cores show strong similarities in glass geochemistry, exemplified by $D^2_{calculated}$ values of 0.97 for major elements and 2.4 for trace elements, both well below the $D^2_{crtiical}$ values of 16.9 and 33.9, respectively. Despite the difference in stratigraphic depths between the two cores, a strong match in sedimentary features above and below each tephra layer is observed (Appendix A.1). The age of deposition of this layer is constrained as less than 17,370 ± 320 cal yr BP, based on a ^{14}C age determination from foraminifera sampled 40 cm below the tephra in core 83PC (Fig. 2, Table 2). Using the sedimentation rate within this core, and following the procedure outlined above, we estimate that deposition of layer V-3 occurred at 13.6 ± 0.5 cal kyr BP. No correlation with a terrestrial deposit was made for this layer.

4.2. Group 2 tephra correlations

Group 2 shards sample tephra from eight spatially adjacent cores within the central study area (cores 77PC, 78PC, 79PC, 31 GC, 32GC, 35GC, 38GC, and 36KC) and all show broadly similar major element composition ranges (Fig. 4) Trace element data, core stratigraphy, and ^{14}C ages, however, demonstrate that the group can be divided into two separate tephra layers (Figs. 5 and 6). The upper tephra (sample# sum137) of core 79PC represents tephra a layer restricted to a single core, V-4. Deposition of the V-4 layer is constrained by ^{14}C ages to be between 2540 ± 110 and 1580 ± 80 cal yr BP in age.

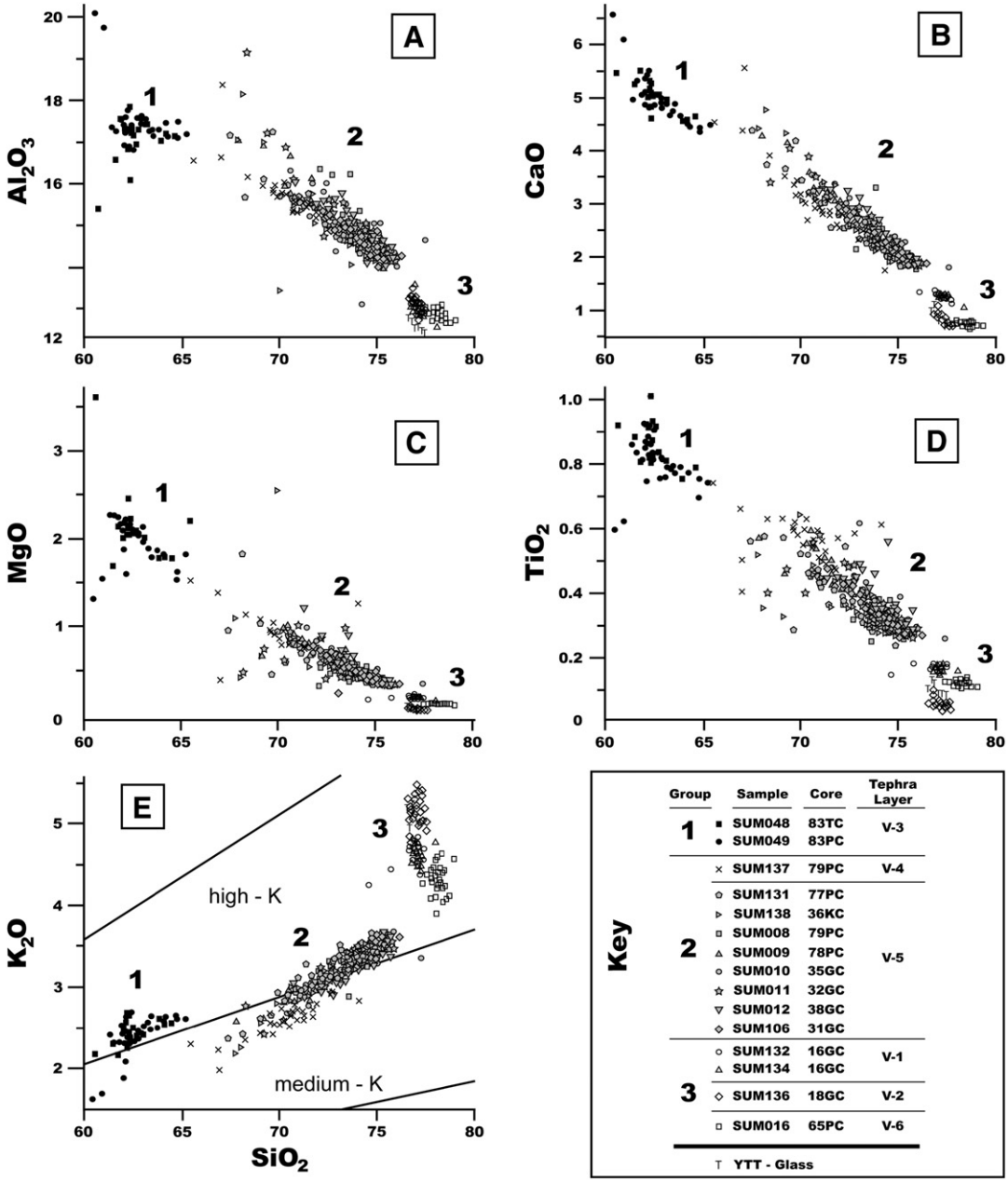

Fig. 4. Binary plots of electron microprobe data of glass shards showing three compositional distinctions. YTT glass compositions from Chesner and Luhr (2010).

We estimate a depositional age of 1.93 ± 0.19 cal kyr BP based on our estimated hemipelagic sedimentation rates.

The deeper tephra (sum008) of 79PC correlates with tephra from seven other cores and denoted as V-5. The eight tephra samples of V-5 are all characterized by major element $D^2_{calculated}$ values below critical (Table 3). With respect to trace elements, $D^2_{calculated}$ values are below critical in all cases with the exception of samples SUM131 and SUM138. These two samples show strong chemical correlation with each other, but are not always characterized by trace element $D^2_{calculated}$ values below critical with the other V-5 tephras. A correlation of these samples with V-5 is, however, suggested by similar trace element compositional trends (Fig. 5c–d), similar values of trace element ratios (Fig. 6) and core stratigraphy constrained by the geophysical data available in the Supplementary appendix (C.1). The trace element compositional differences within V-5 may be attributed to crystal fractionation, post-depositional processes, or analytical variability. Shard morphologies and sizes are similar (micropumiceous, 110–90 μm) within all Group 2 tephras with the exception of SUM138, which is characterized by a predominance of smaller (~30 μm), platy shards.

The V-5 layer represents the most widespread and best chronological constraint of this study. Foraminifera sampled directly above and below tephra sample SUM008 within Core 79PC bracket the depositional age between 4690 ± 100 and 4860 ± 60 cal yr BP. This age is consistent with the tephra (sample# SUM131) within core 77PC, which is bracketed by ^{14}C ages of 7030 ± 100 and 2980 ± 110 cal yr BP. Age control is unavailable for the other cores that contain V-5 cores from within the Sunda trench.

No known eruption is documented from Sumatra that might correlate with the V-5 tephra layer. Compositional glass data from 1883 Krakatau tephra (Mandeville et al., 1996) and the pre-1883 tephra preserved in marine sediments (Beauregard, 2001) did not match any from the present study.

Group 2 tephras (V-4 and V-5) do show broad major element similarity with the older, Pleistocene dacitic tephras from the Sunda straight marine tephras (Fig. 1) identified by Ninkovich (1979), although the

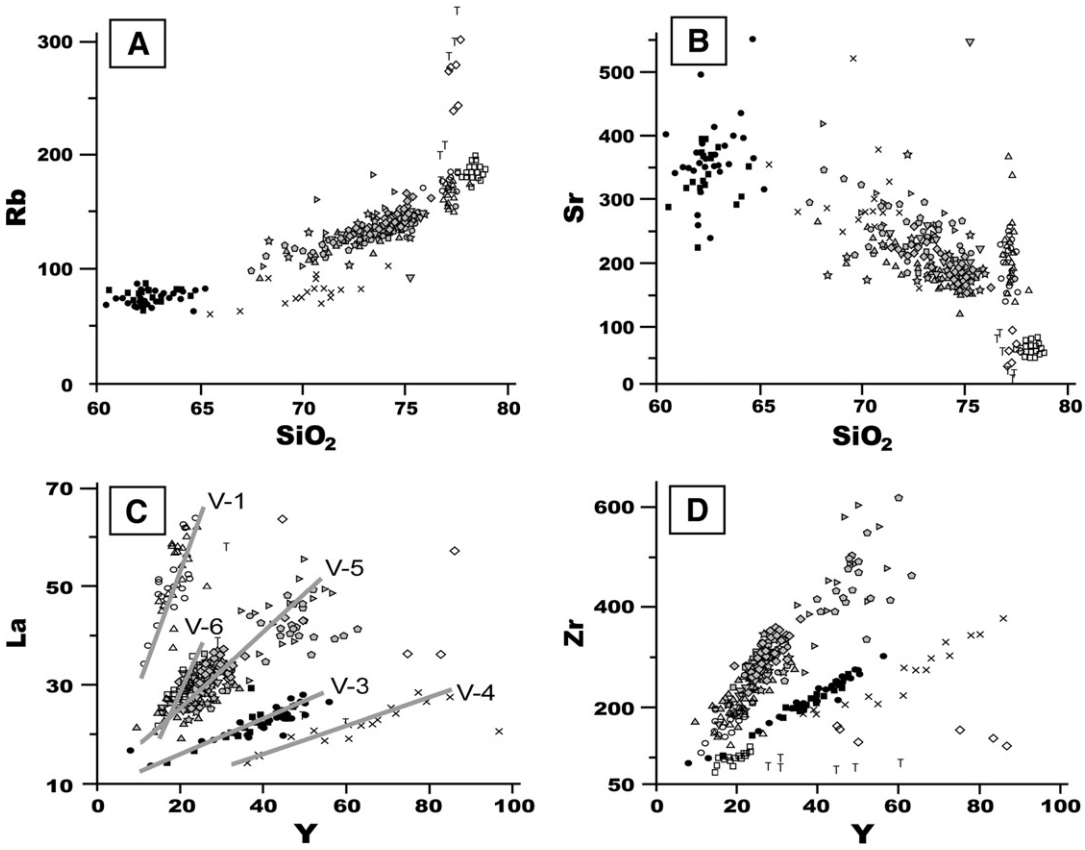

Fig. 5. Binary plots of select trace element compositions. (A) Rb and (B) Sr are among the few elements to show compositional trends with increasing silica. High field strength elements such as La and Zr and Y show strong correlation (C and D) with each other demonstrating the distinction of the tephra layers of this study. Symbols are the same as in Fig. 4.

large geographic distance between these cores (>850 km) suggests different magmatic sources. A likely source of the V-4 and V-5 tephras is the highly active volcanoes of the Padang Highlands of central Sumatra. Marapi is the most historically active Sumatran volcano with more than 50 small-to-moderate explosive eruptions recorded since the end of the 18th century (Smithsonian Institution, 2011) and should be singled out for detailed study. However, limited available data from Marapi terrestrial tephras (M. del Marmol, personal communication) indicate more mafic compositions (SiO_2 as low as 54 wt.%) than those of this study.

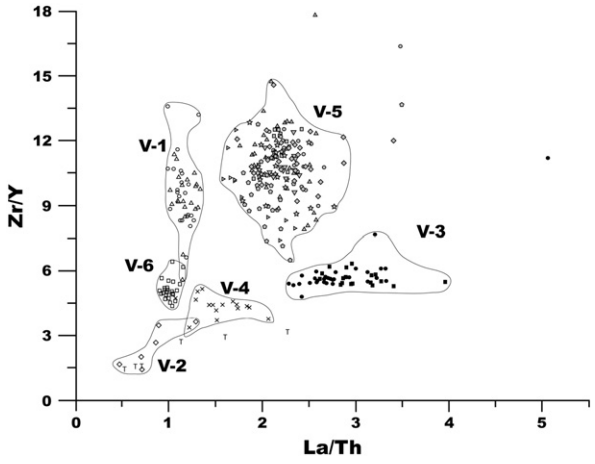

Fig. 6. Zr/Y vs. La/Th showing the clear compositional distinctions among the six tephra layers identified in this study. Symbols are the same as in Figs. 4 and 5. Outliers omitted from group outlines.

4.3. Group 3 tephra correlations

The four tephra samples of Group 3 (cores 65PC, 18GC, 16GC) are separated into three units based on trace element compositions (Figs. 4–6) and core stratigraphy. Although the two tephra deposits within core 16GC are separated by a ~12 cm sequence of silt to very fine sand turbidites (Fig. 2, Appendix A.1), we interpret the tephras as a single layer, V-1. Glass shards from the two tephra samples (SUM132 and SUM134) in this core are chemically indistinguishable ($D^2_{calculated}$ values of 0.53 for major elements and 2.5 for trace elements), and a lack of hemipelagic sediment between the tephras suggests that the turbidites were deposited rapidly between depositions of the two tephra. The turbidites contain Bouma c and d beds (Bouma, 1962) and are consistent with deposition following tectonic seismicity. This scenario is consistent with an eruption coinciding with turbidite-producing seismicity and may imply a relationship between the two events (e.g. Linde and Sacks, 1998). No absolute ages constrain the deposition of V-1. Using a sedimentation rate extrapolated from 18GC, we estimate a depositional age of ~31 ka for V-1.

Tephra sampled from core 18GC, less than 3 km from V-1 (16GC) in the northern part of the study area, is interpreted as a unique tephra layer, named V-2. Despite the proximity, neither layer (V-1 nor V-2) was found in its neighboring core and demonstrates that not all tephras are preserved in the depositional record in these dynamic marine environments. Glass shards from V-2 are the smallest (≤30 μm) analyzed in this study, necessitating a smaller laser ablation spot size (30 μm) and less-precise trace element LA-ICP-MS analyses from fewer (6) shard measurements. However, major element data collected by EMPA, using a 10 μm spot size, clearly distinguish this layer from other Group 3 tephras (Fig. 4). No direct ages are available below layer V-2; a sedimentation-rate derived age of ~110 ka is calculated based on the

overlying ages (Fig. 2). As discussed in Section 3.2, there is unconstrained error involved in the sedimentation rate and the glass compositional data support a correlation with the YTT. Age estimates for the YTT range from 68 ± 7 to 81 ± 17 kyr BP, with a preferred age of 74 ± 2 kyr BP (Oppenheimer, 2002). Glass shards from V-2 show compositional similarity with published major element glass compositions of the YTT (Ninkovich et al., 1978; Ninkovich, 1979; Dehn et al., 1991; Shane et al., 1995; Chesner, 1998; Pattan et al., 1999; Bühring and Sarnthein, 2000; Chesner and Luhr, 2010) and trace element data from glass shards analyzed by Chesner and Luhr (2010) reveal $D^2_{calculated}$ values below critical for 22 trace elements (Table 3). Given that the depositional age of V-2 is not directly constrained by ^{14}C ages, we consider it likely that the V-2 correlates with the YTT. There is no evidence that any of the other cores analyzed in the current study reached the depth of the YTT.

Layer V-6 is identified within a single core (65PC) that was sampled near the Sunda trench off the coast of southern Sumatra and is characterized by the highest silica concentrations (77–79 wt.%) of glass measured in this study. V-6 shows evidence for a complex depositional history; the lowest half-meter of core 65PC contains a sequence of reworked tephras (Appendix A.1). Based on stratigraphy, foraminifera abundance, and degree of bioturbation, we interpret the entire sequence as belonging to deposition of tephra from a single eruptive episode interrupted by upslope volcaniclastic turbidite deposition. The volcaniclastic turbidites were likely triggered by upslope sediment loading shortly (days to years) following primary deposition. The sequence is capped by ~35 cm of volcaniclastic turbidites. Six tephra samples (two primary and four reworked) were analyzed within the sequence and all consist of glass shards with near-identical major element compositions ($D^2_{calculated}$ values < 2.4). Trace element data was collected for sample SUM016 only. No absolute ages are available for this slope core at the time of this publication. Using a sedimentation rate calculated from nearby slope cores 61PC, 63PC, and 67PC (distanced 207, 135, and 135 km respectively from 65PC), we estimate a depositional age of ~27.5 ka for V-6. Although there is no clear terrestrial unit that correlates with this tephra, the highly silicic composition of glass from V-6 is likely related to the ignimbrite-producing region of south Sumatra (Westerveld, 1952; Ninkovich, 1979; Gasparon, 2005).

4.4. Implications

Given the scarcity of data concerning the Late Pleistocene to Holocene eruptive history of Sumatra, it is not surprising that we were unable to correlate the majority of the marine tephras of this study with their terrestrial sources. Our data, thus, provide an opportunity to provide some of the first constraints on the explosive eruptive history of the region during this timeframe. We suggest that at least five previously undocumented explosive eruptions are documented within the deep-sea marine cores sampled in this study with eruption ages of approximately 30.9, 27.5, 13.6, 4.9, and 1.9 ka. The minimum eruption interval of ~6.2 thousand years preserved within these cores is considerably shorter than the ~414 k.y. interval between 2.5 Ma and 73.5 ka for eruptions producing >1 cm of tephra at a distance of ~1000 km (VEI ≥ 5) northwest of northern Sumatra calculated by Dehn et al. (1991); and considerably longer than the historic small-to-moderate eruptions (VEI ≤ 3) that occur on a yearly to decadal scale.

Calculation of eruptive volumes represented by the tephra layers identified in this study is complicated by the lack of dispersal data and unknown terrestrial sources. In an attempt to establish absolute minimum eruptive volumes, we apply the empirical equation of Legros (2000) for calculating eruptive volumes where only a single isopach is available:

$$\text{Minimum volume}(V_{min}) = 3.69 * \text{thickness} * \text{ellipse area}.$$

Table 5
Minimum volume estimates of individual tephra units.

Tephra unit	Distance[a] (km)	Ellipse short:long	Ellipse area (km^2)	Layer thickness (cm)	V_{min}[b] (km^3)	VEI
V-1	310	0.25	18,869	9.0	6.3	5
V-2	310	0.25	18,869	5.0	3.5	5
V-3	250	0.25	12,272	1.3	0.6	4
V-4	280	0.25	15,394	3.5	2.0	5
V-5[c]	285	0.25	15,948	8.0	4.7	5
V-6	210	0.25	8659	18.0	5.8	5

[a] Distance is core location to nearest arc volcano.
[b] $V_{min} = 3.79 * \text{thickness} * \text{ellipse area}$.
[c] The volume increases to 5.2 km^3 considering a second ellipse as described in the text.

The minimum distribution for four of the newly documented tephra layers is estimated by a major axis equal to the distance from the core site to the nearest Sumatran arc volcano and a minor axis ¼ of this length. The wider distribution of V-5 allows for a slightly larger ellipse width. The minimum ellipse areas calculated in this study are considered conservative in comparison to the majority of areal distributions of tephra described elsewhere (e.g. Fisher and Schmincke, 1984) and do not factor wind direction. Today, lower troposphere wind direction near Sumatra is westerly to southwesterly in boreal summer and northeasterly in the winter (Krishnamurti, 1987), suggesting that the tephras of this study primarily preserve summer eruptions. The results of the V_{min} calculation range from 0.6 to 6.3 km^3 (V.E.I. 4–5, Table 5). As the widespread V-5 tephra layer was identified in multiple cores along 110 km of the trench axis, the minimum volume for this layer is calculated using the above equation with the 8.0 cm layer within core 79PC (4.7 km^3) and adding a wider ellipse that encompasses the correlated trench cores (Fig. 1) with an average thickness of 2.2 cm (0.5 km^3) for a total V_{min} of 5.2 km^3. The minimum volume for V-1 is calculated using the sum of the two tephras in core 16GC producing a V_{min} of 6.3 km^3, the largest volume of this study. Considering the two layers separately produces minimum volumes of 2.8 and 3.5 km^3. Our estimate for the V-6 volume varies with the interpretation of the volcaniclastic-turbidite sequence. The sum thickness of the four primary tephras is 18 cm and corresponds to a V_{min} of 5.8 km^3. Considering each of the four primary tephras separately corresponds to minimum volumes of 1.9, 1.6, 0.7, and 1.5 km^3.

The three youngest tephra layers (V-3, V-4, V-5) identified in this study were collected in the central study region suggesting that central Sumatra may be the source area for the most frequent, large explosive eruptions. This suggests that central Sumatra should be subject to further terrestrial studies to identify the most frequently active volcanoes and their associated hazards.

5. Conclusions

In this study we have identified five newly discovered marine tephra layers and one occurrence of the YTT within, and adjacent to, the Sunda trench west of the island of Sumatra. No correlations with terrestrial deposits are known, although the most likely source is considered the western Sunda arc of Sumatra. Primary tephra thicknesses range from 1.3 to 18 cm. A conservative approach to volume estimates reveals that the newly erupted tephras correspond to eruptive volumes of at least 0.6 to 6.3 km^3. Tephra layer V-5 represents the most widespread tephra and correlates with eight cores taken offshore of central Sumatra. ^{14}C age determinations of this tephra within the slope cores that contain foraminifera tightly constrain the deposition at ~4.9 ka. A younger eruption from the central region, layer V-4, was deposited ~1.9 ka and suggests central Sumatra as a location of frequent explosive eruptions capable of transporting centimeters of ash to distances greater than 280 km. Layer V-3, also offshore central Sumatra, does not have

direct age control but hemipelagic sedimentation rate estimates suggests deposition ~13.6 ka. A close relation between the primary tephra of V-1 and turbidites in the northern region of the study is suggestive of coincident volcanic eruptions from the arc front and seismicity along the plate boundary. In the southern study area, layer V-6 also shows evidence for a complex depositional history at ~27.5 ka, although this age is constrained only by sedimentation rate estimates. Further research is recommended for much of the western Sunda arc of Sumatra, and we highlight the central Sumatra region as particularly at risk of large explosive eruptions.

Acknowledgments

This research was supported by the United States National Science Foundation, through grants to CG and AJRK (NSF-OCE-0526655). Andy Ungerer assisted with laser ablation analyses; Frank Tepley and Dale Burns provided assistance with electron microprobe analyses. We thank M. del Marmol for data from Marapi. A thorough review by Andrei M. Sarna-Wojcicki and an anonymous reviewer resulted in a significantly improved manuscript. We thank Ann E. Morey, Sarah Strano, Amy M. Garrett, and Jeff Beeson for assisting with radiocarbon sampling and radiocarbon material preparation.

Appendix A. Supplementary data

Supplementary data associated with this article can be found in the online version, at http://dx.doi.org/10.1016/j.jvolgeores.2012.03.007. These data include Google maps of the most important areas described in this article.

References

Adams, J., 1990. Paleoseismicity of the Cascadia subduction zone: evidence from turbidites off the Oregon–Washington margin. Tectonics 9 (4), 569–583.
Beauregard, J.L., 2001, Explosive rhyodacitic volcanism: the evolution and frequency of pre-1883 eruptions at Krakatau volcano, Indonesia. Ph.D. thesis, University of Rhode Island.
Bellier, O., Sébrier, M., 1994. Relationship between tectonism and volcanism along the Great Sumatran Fault Zone deduced by SPOT image analyses. Tectonophysics 233 (3-4), 215–231.
Bellier, O., Bellon, H., Sébrier, M., Sutanto, Maury, R.C., 1999. K–Ar age of the Ranau Tuffs: implications for the Ranau caldera emplacement and slip-partitioning in Sumatra (Indonesia). Tectonophysics 312, 347–359.
Bellon, H., Maury, R.C., Sutanto, Soeria-Atmadja, R., Cotton, J., Polve, M., 2004. 65 m.y.-long magmatic activity in Sumatra (Indonesia), from Paleocene to present. Bulletin De La Société Géologique de France 175 (1), 61–72.
Bouma, A.H., 1962. Sedimentology of Some Flysch Deposits: A Graphic Approach to Facies Interpretation. Elsevier, Amsterdam. 168 pp.
Bronk Ramsey, C., 2009. Bayesian analysis of radiocarbon dates. Radiocarbon 51 (1), 337–360.
Bühring, C., Sarnthein, M., 2000. Toba ash layers in the South China Sea: evidence of contrasting wind directions during eruption ca. 74 ka. Geology 28 (3), 275–278.
Chesner, C.A., 1998. Petrogenesis of the Toba Tuffs, Sumatra, Indonesia. Journal of Petrology 39 (3), 397–438.
Chesner, C.A., Luhr, J.F., 2010. A melt inclusion study of the Toba Tuffs, Sumatra, Indonesia. Journal of Volcanology and Geothermal Research 197 (1–4), 259–278.
Chesner, C.A., Rose, W.I., Deino, A., Drake, R., Westgate, J.A., 1991. Eruptive history of Earth's largest Quaternary caldera (Toba, Indonesia) clarified. Geology 19 (3), 200–203.
Dehn, J., Farrell, J.W., Schminke, H.U., 1991. Neogene tephrochronology from Site 758 on northern Ninetyeast Ridge: Indonesian arc volcanism of the past 5 MA. In: Weissel, J., Peirce, J., et al. (Eds.), Proceedings of the Ocean Drilling Program, Scientific Results, College Station Texas, Ocean Drilling Program, 271, pp. 273–295.
Fisher, R.V., Schmincke, H.U., 1984. Pyroclastic Rocks. Springer-Verlag, Berlin. 472 pp.
Gasparon, M., 2005. Chapter 9: Quaternary volcanicity. In: Barber, A.J., Crow, M.J., Milsom, J. (Eds.), Sumatra: Geology, Resources and Tectonic Evolution: Geological Society, London, Memoir, 31, pp. 120–130.
Gasparon, M., Varne, R., 1995. Sumatran granitoids and their relationship to Southeast Asian terranes. Tectonophysics 251, 277–299.
Kent, A.J.R., Stolper, E.M., Francis, D., Woodhead, J., Frei, R., Eiler, J., 2004. Mantle heterogeneity during the formation of the North Atlantic Tertiary Province: constraints from trace element and Sr–Nd–Os–O isotope systematics of Baffin Island picrites. Geochemistry, Geophysics, Geosystems 5, Q11004, http://dx.doi.org/10.1029/2004GC000743.
Krishnamurti, T.N., 1987. Monsoon models. In: Fein, J.S., Stephens, P.L. (Eds.), Monsoons. John Wiley & Sons, New York, pp. 467–522.
Legros, F., 2000. Minimum volume of a tephra fallout deposit estimated from a single isopach. Journal of Volcanology and Geothermal Research 96, 25–32.
Linde, A.T., Sacks, I.S., 1998. Triggering of volcanic eruptions. Nature 395, 888–890.
Mandeville, C.W., Carey, S., Sigurdsson, H., 1996. Magma mixing, fractional crystallization and volatile degassing during the 1883 eruption of Krakatau volcano, Indonesia. Journal of Volcanology and Geothermal Research 74, 243–274.
Newhall, C.G., Self, S., 1982. The volcanic explosivity index (VEI): an estimate of explosive magnitude for historical volcanism. Journal of Geophysical Research 87, 1231–1238.
Ninkovich, D., 1976. Late Cenozoic clockwise rotation of Sumatra. Earth and Planetary Science Letters 29, 269–275.
Ninkovich, D., 1979. Distribution, age and chemical composition of tephra layers in deep-sea sediments off western Indonesia. Journal of Volcanology and Geothermal Research 5, 67–86.
Ninkovich, D., Donn, W.L., 1976. Explosive Cenozoic volcanism and climatic implications. Science 194, 899–906.
Ninkovich, D., Sparks, R.S.J., Ledbetter, M.T., 1978. The exceptional magnitude and intensity of the Toba eruption, Sumatra: An example of the use of deep-sea tephra layers as a geological tool. Bulletin Volcanologique 41, 286–298.
Oppenheimer, C., 2002. Limited global change due to the largest known Quaternary eruption, Toba ≈ 74 kyr BP? Quaternary Science Reviews 21, 1593–1609.
Pattan, J.N., Shane, P., Banakar, V.K., 1999. New occurrence of Youngest Toba Tuff in abyssal sediments of the Central Indian Basin. Marine Geology 155, 243–248.
Patton, J.R., Goldfinger, C., Morey, A., Erhardt, M., Black, B., Garrett, A.M., et al., 2010. Temporal clustering and recurrence of Holocene paleoearthquakes in the region of the 2004 Sumatra-Andaman earthquake. Seismological Research Letters 81, 290.
Pearce, N.J.G., Denton, J.S., Perkins, W.T., Westgate, J.A., Alloway, B.V., 2007. Correlation and characterization of individual glass shards from tephra deposits using trace element laser ablation ICP-MS analyses: current status and future potential. Journal of Quaternary Science 22 (7), 721–736.
Pearce, N.J.G., Alloway, B.V., Westgate, J.A., 2008. Mid-Pleistocene silicic tephra beds in the Auckland region, New Zealand: their correlation and origins based on trace element analyses of single glass shards. Quaternary International 178, 16–43.
Perkins, M.E., Nash, W.P., Brown, F.H., Fleck, R.J., 1995. Fallout tuffs of Trapper Creek, Idaho — a record of Miocene explosive volcanism in the Snake River Plain volcanic province. GSA Bulletin 107 (12), 1485–1506.
Perkins, M.E., Brown, F.H., Nash, W.P., McIntosh, W., Williams, S.K., 1998. Sequence, age, and source of silicic fallout tuffs in middle to late Miocene basins of the northern Basin and Range province. GSA Bulletin 110 (3), 334–360.
Reimer, P.J., Baillie, M.G.L., Bard, E., Bayliss, A., Beck, J.W., Blackwell, P.G., Bronk Ramsey, C., Buck, C.E., Burr, G.S., Edwards, R.L., Friedrich, M., Grootes, P.M., Guilderson, T.P., Hajdas, I., Heaton, T.J., Hogg, A.G., Hughen, K.A., Kaiser, K.F., Kromer, B., McCormac, F.G., Manning, S.W., Reimer, R.W., Richards, D.A., Southon, J.R., Talamo, S., Turney, C.S.M., van der Plicht, J., Weyhenmeyer, C.E., 2009. IntCal09 and Marine09 radiocarbon age calibration curves, 0–50,000 years cal BP. Radiocarbon 51 (4), 1111–1150.
Rock, N.M.S., Syah, H.H., Davis, A.E., Hutchison, D., Styles, M.T., Lena, R., 1982. Permian to Recent volcanism in northern Sumatra, Indonesia: a preliminary study of its distribution, chemistry, and peculiarities. Bulletin of Volcanology 45 (2), 127–152.
Rose, W.I., Chesner, C.A., 1987. Dispersal of ash in the great Toba eruption, 75 ka. Geology 15, 913–917.
Shane, P., Westgate, J., Williams, M., Korisettar, R., 1995. New geochemical evidence for the Youngest Toba Tuff in India. Quaternary Research 44, 200–204.
Smith, W.H.F., Sandwell, D.T., 1997. Global sea floor topography from satellite altimetry and ship depth soundings. Science 277, 1957–1962.
Smithsonian Institution, 2012. Global Volcanism Program. http://www.volcano.si.com.
Song, S.R., Chen, C.H., Lee, M.Y., Yang, T.F., Iizuka, Y., Wei, K.Y., 2000. Newly discovered eastern dispersal of the youngest Toba Tuff. Marine Geology 167, 303–312.
Stuiver, M., Braziunas, T.F., 1993. Modeling atmospheric ^{14}C influences and ^{14}C ages of marine samples to 10,000 BC. Radiocarbon 35 (1), 137–189.
Stuiver, M., Polach, H.A., 1977. Discussion: reporting of ^{14}C data. Radiocarbon 19 (3), 355–363.
Stuiver, M., Reimer, P.J., Braziunas, T.F., 1998. High-precision radiocarbon age calibration for terrestrial and marine samples. Radiocarbon 40 (3), 1127–1151.
Taylor, R.E., Stuiver, M., Reimer, P.J., 1996. Development and extension of the calibration of the radiocarbon time scale: archaeological applications. Quaternary Science Reviews 15, 655–668.
Ukstins Peate, I., Baker, J.A., Kent, A.J., Al-Kadasi, M., Al-Subbary, A., Ayalew, D., Menzies, R., 2003. Correlation of Indian Ocean tephra to individual Oligocene silicic eruptions from Afro-Arabian flood volcanism. Earth and Planetary Science Letters 211 (3-4), 311–327.
Ukstins Peate, I., Baker, J.A., Al-Kadasi, M., Al-Subbary, A., Knight, K.B., Riisager, P., Thirlwall, M.F., Peate, D.W., Renne, P.R., Menzies, M.A., 2005. Volcanic stratigraphy of large-volume silicic pyroclastic eruptions during Oligocene Afro-Arabian flood volcanism in Yemen. Bulletin of Volcanology 68, 135–156.
van Bemmelen, R.W., 1949. The Geology of Indonesia and Adjacent Archipelago. Government Printing Office, The Hague.
Westerveld, J., 1952. Quaternary volcanism on Sumatra. GSA Bulletin 63, 561–594.
Whitford, D.J., 1975. Strontium isotopic studies of the volcanic rocks of the Sunda arc, Indonesia, and their petrogenetic implications. Geochimica et Cosmochimica Acta 39, 1287–1302.